Length-dependent self-assembly of oligothiophene derivatives in thin films

Brian S. Rolczynski
Department of Chemistry, Northwestern University, Evanston, Illinois 60208; Chemical Sciences and Engineering Division and Argonne National Laboratory, Argonne, Illinois 60439; and Argonne-Northwestern Solar Energy Research (ANSER) Center, Northwestern University, Evanston, Illinois 60208

Jodi M. Szarko
Department of Chemistry, Northwestern University, Evanston, Illinois 60208; and Argonne-Northwestern Solar Energy Research (ANSER) Center, Northwestern University, Evanston, Illinois 60208

Byeongdu Lee and Joseph Strzalka
X-ray Sciences Division, Argonne National Laboratory, Argonne, Illinois 60439

Jianchang Guo
Chemical Sciences and Engineering Division and Argonne National Laboratory, Argonne, Illinois 60439; and Department of Chemistry and The James Franck Institute, The University of Chicago, Chicago, Illinois 60637

Yongye Liang
Department of Chemistry and The James Franck Institute, The University of Chicago, Chicago, Illinois 60637

Luping Yu[a)]
Argonne-Northwestern Solar Energy Research (ANSER) Center, Northwestern University, Evanston, Illinois 60208; and Department of Chemistry and The James Franck Institute, The University of Chicago, Chicago, Illinois 60637

Lin X. Chen[a)]
Department of Chemistry, Northwestern University, Evanston, Illinois 60208; Chemical Sciences and Engineering Division and Argonne National Laboratory, Argonne, Illinois 60439; and Argonne-Northwestern Solar Energy Research (ANSER) Center, Northwestern University, Evanston, Illinois 60208

(Received 6 May 2010; accepted 4 August 2010)

Thin-film aggregation characteristics of a series of oligothiophenes with a central thieno[3,4-b] thiophene ester unit and 4 (M5), 8 (M9), and 16 (M17) regioregular hexylthiophene units were investigated. These oligomers exhibited length-dependent self-assembly characteristics upon spin coating. M9 formed long fibers, while M5 and M17 formed random domains. Grazing incidence x-ray diffraction was performed to understand the reason for this length dependence. The M5 had a dominant ester–ester interaction that disrupted long-range order. The M9 morphology was due to a balance of orthogonal backbone and ester effects, which imposed long-range order on the M9 aggregates. Meanwhile, the M17 ester chain had a smaller relative contribution to packing and functioned as a molecular defect, disrupting long-range order. As a result, though the local self-assembly between monomers was very similar for the molecules, backbone length dependent changes in intermolecular forces dominated long-range structure. The analysis of self-assembly characteristics in these materials provides guidance in the design of organic conjugated materials for use in semiconductor devices.

I. INTRODUCTION

The π-conjugated organic molecules are important building blocks for lightweight, highly tunable,[1] cost-effective,[2] and easily processed[3] materials used in devices such as organic field effect transistors (OFETs), organic light-emitting diodes (OLEDs), and organic photovoltaic (OPV) cells.[4] However, one serious challenge in the design of these materials lies in understanding how molecular structure can affect the packing morphology in films and, furthermore, the device performance. The key process in film fabrication is self-assembly, a process of balancing different interactions to assemble molecules spontaneously into desirable packing structures, such as interpenetrating networks.[5] Despite much progress in the investigation of organic film aggregation,[6–9] there is yet to be a comprehensive, predictable understanding of how molecules will aggregate based on their molecular structure. To develop this understanding, it is necessary to expand the list of known structure interactions, and

[a)]Address all correspondence to these authors.
e-mail: lchen@anl.gov; lupingyu@uchicago.edu
DOI: 10.1557/jmr.2010.14

especially to explain systems where unexpected aggregation behaviors are observed, to deduce new supramolecular design strategies.

Organic semiconductor device performance depends heavily on molecular assembly architectures in active layers,[10,11] which determine largely the function of related properties of the films, such as exciton splitting efficiency, exciton/charge-carrier mobility, and emission or light-harvesting quantum yields.[12,13] Frequently, one can design a targeted molecular packing architecture for specific functions, but the targeted self-assembly architecture may not be easily achievable in reality. Two main reasons for the uncertainty are the interplay of different forces between molecules and with solvent effects. For example, self-assembly between conjugated polymer chains is assisted by interactions between aliphatic side chains and between π-conjugated backbones, which facilitates alternating aromatic and aliphatic layers.[14] As a result, oligothiophenes with these side chains form stacked linear arrays along the aliphatic side-chain direction, whereas oligothiophenes without these side chains form herringbone structures.[15,16] Such segregated morphologies affect the exciton and energy-transport properties of organic active layers in semiconductor devices.[17] Because self-assembled morphology plays such an important role in electronic properties, derivatives of benchmark electronic organic molecules must be designed to optimize the film morphology as well as the photophysical characteristics.[18] Meanwhile, a bulk, micrometer-scale order facilitates efficient, long-range transportation of charge carriers.[19,20] This can also greatly affect overall performance of the devices, such as the power conversion efficiency (PCE) of solar cells.[11] For example, we have recently discovered a unique packing orientation for a novel high PCE organic photovoltaic (OPV) polymer system[21] that has conjugated polymer backbone planes parallel to the electrode surface and contributes greatly to the record PCE of ~8% in OPV devices.

In this report, we present our investigation on the self-assembly of a system of diblock oligomers consisting of an oligothiophene (T) backbone with a central thieno [3,4-b]thiophene (TT) unit, which we collectively call the M series (Fig. 1).[22] The oligomers under investigation are M5, M9, and M17, which have 4, 8, and 16 T units, respectively. These diblock oligomers were synthesized to model a series of low band gap conjugated polymers for OPV applications with the same constituents and stoichiometry.[1] To our surprise, when spin coated into films, members of this oligomer series formed assemblies with very different morphologies. Although it is well known that major substitutions to the chemical structure lead to a change in the aggregation characteristics of organic molecules,[6] it is unclear how other differences, such as oligomer backbone length, lead to drastically different morphologies in thin films on a variety of spatial scales. In

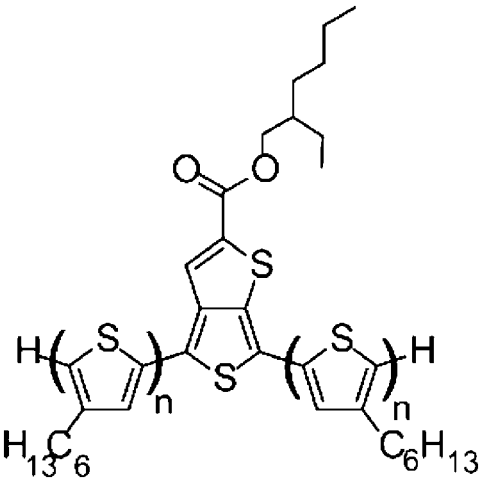

FIG. 1. The M series, consisting of M5 ($n = 2$), M9 ($n = 4$), and M17 ($n = 8$).

our previous studies,[22] we have found both experimental and theoretical evidence that the central TT unit with an ester group draws electron density toward the center of the oligomer in the excited state, through a pseudocharge-transfer (PCT) transition from HOMO to LUMO. This PCT is responsible for the low band gap in the corresponding polymers. The band gap of the oligomers can also be tuned by varying the number of T units in the oligomers, but the morphology of the films in terms of molecular packing is also a function of the oligomer length as discovered in our study. Therefore, we present the structural details through the grazing incidence x-ray diffraction (GIXRD) results in this study to identify the morphological control factors that eventually may allow us to establish correlations in molecular structure and film morphology. These oligomers are referenced to poly (3-hexylthiophene) (P3HT) that, except for the thieno [3,4-b]thiophene ester moiety, is the long backbone length analog of the M series. The asymmetry that this moiety imposes on the side-chain axis is considered in two scenarios: (i) when it functions as a regular feature in crystallization as part of a shorter oligomer and (ii) when it disrupts long-range ordering as a molecular defect to the P3HT template in a longer oligomer.

II. EXPERIMENTAL METHODS

The synthesis of the M series oligomers is described in Ref. 1 and in the Supporting Information of Ref. 21. Thin-film samples of the M series shown in Fig. 1 were prepared from 10 mg/mL solutions in chloroform and spin-coated on glass (for AFM studies) or silicon substrates (for GIXRD studies) at 1000 rpm for 1 min. No further treatment, such as annealing, was applied. Morphologies of M9 and M17 thin films were found to be consistent

for >1 year in atmospheric conditions. The M5 films beaded up soon after spin coating and did not present evidence of regular order in the GIXRD experiments.

Atomic force microscopy (AFM) was performed in atmosphere using a PicoSPM (Agilent Technologies, Santa Clara, CA) in alternating-current (AC) mode with a 300 kHz silicon-tip probe.

Geometry optimization for the M series oligomers in vacuum was performed in Hyperchem (Hypercube, Inc., Gainesville, FL) by initially energy minimizing with the MM+ force field, then with MNDO because it handles sulfur-containing conjugated molecules better than other methods.[23] The molecules were initially built with flat backbones and fully extended oligomer chains.

GIXRD, or GIWAXS (grazing incidence wide angle x-ray scattering) and GISAXS (grazing incidence small angle x-ray scattering), experiments were performed at Beamlines 12BM (for GIWAXS) and 8ID (for GISAXS) in the Advanced Photon Source (APS) in Argonne National Laboratory. In these techniques, a synchrotron-generated x-ray beam is incident on the sample surface at a small angle relative to the surface plane. Based on the *d*-spacing of assemblies in the sample, x-rays are diffracted to positions on a two-dimensional MAR detector. These diffraction patterns are used to deduce the self-assembly characteristics of the sample. With this technique, it is possible to obtain unit-cell dimensions for polycrystalline samples, which are common in spin-coated thin films, as well as to gain insights about the assembled domains through analysis of the smearing of the diffraction peaks. The x-ray photon energy for these experiments was 8 keV, and the detector-to-sample distances for GISAXS and GIWAXS were 1308 and 285 mm, respectively. The beam at 12BM was focused by a toroidal mirror, making it difficult to quantify the exact uncertainty of diffraction measurements because the beam was uncollimated. The incident x-ray beam was approximately 1 × 1 mm at Beamline 12BM, and 100 μm tall by 50 μm wide at Beamline 8ID. Because of the grazing incidence geometries, the footprint of these beams was centimeters long on the sample surface.

Because the x-rays are diffracted according to the *d*-spacing of electron density rich features, the distance between TT ester fragments and between T backbones generate the strongest signals. Additionally, the diffraction signal differentiates between interactions occurring out-of-plane (*z* direction) and in-plane (*xy* direction) with respect to the substrate surface. By convention, the out-of-plane direction corresponds to the *a* unit-cell parameter, while the in-plane direction corresponds to the *b* and *c* parameters. For this system, *a* denotes the side-chain axis, *b* corresponds to the π-stacking axis, and *c* represents the conjugated backbone length axis. The *d*-spacing of a crystallographic plane is calculated by using the Bragg equation, $d = 2\pi/q$.[24]

III. RESULTS AND DISCUSSION

Calculated molecular geometries are summarized in Fig. 2. The length of the straightened ester chain was 9.6 Å. The calculations converged at energy gradients of -5.97×10^4 kJ/mol for M5, -1.05×10^5 kJ/mol for M9, and -1.85×10^5 kJ/mol for M17. The energy minimization processes retained fully extended aliphatic chains and disrupted the planarity of the conjugated oligomer backbones by causing an alternating forward and backward tilt of each monomer. However, in thin films the backbones are expected to be flattened.[25]

The AFM images for the three oligomers with different backbone lengths showed distinct morphologies in thin films (Fig. 3). The most striking observation is the long fibrous morphology only appearing in M9 with two distinct dimensions: wider crystalline fibers roughly 0.8 to 1.2 μm wide and >26 μm long, and thinner fibrils roughly 80 to 100 nm in width (Fig. 2). The thickness of the larger fibers is approximately 20 nm. In contrast, the films of M5 and M17 both show domains without apparent order. The random domains in M5 are approximately 150 to 300 nm in diameter, while those in M17 are approximately 75 to 300 nm in size. The main questions are therefore (i) why does the fibrous morphology only appear in a particular oligomer length of M9 and not in related oligomers with shorter or longer length, (ii) what are the forces involved in self-assembly processes, and (iii) what are the implications for the control of materials morphology in specific applications and functions?

To understand why these oligomers exhibit such different, length-dependent film morphologies, GIXRD measurements were carried out to probe molecular packing in these self-assembled architectures at different levels, from local structures to packing domains. We focus on the backbone-length dependence and the interplay of different forces during packing.

The GIXRD patterns for the oligomers can be obtained in different *q* ranges via GIWAXS and GISAXS studies,

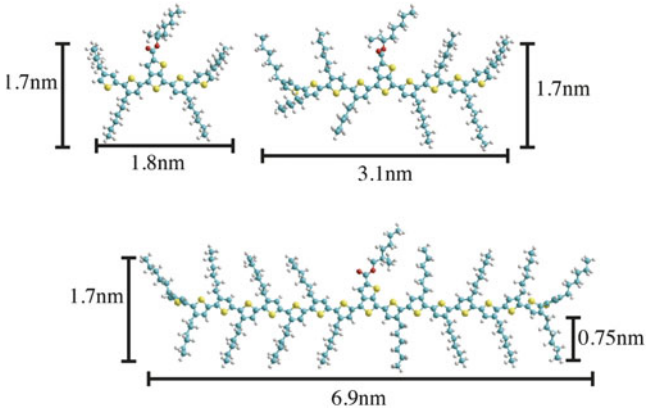

FIG. 2. MNDO geometry-optimized dimensions are indicated for M5 (a), M9 (b), and M17 (c).

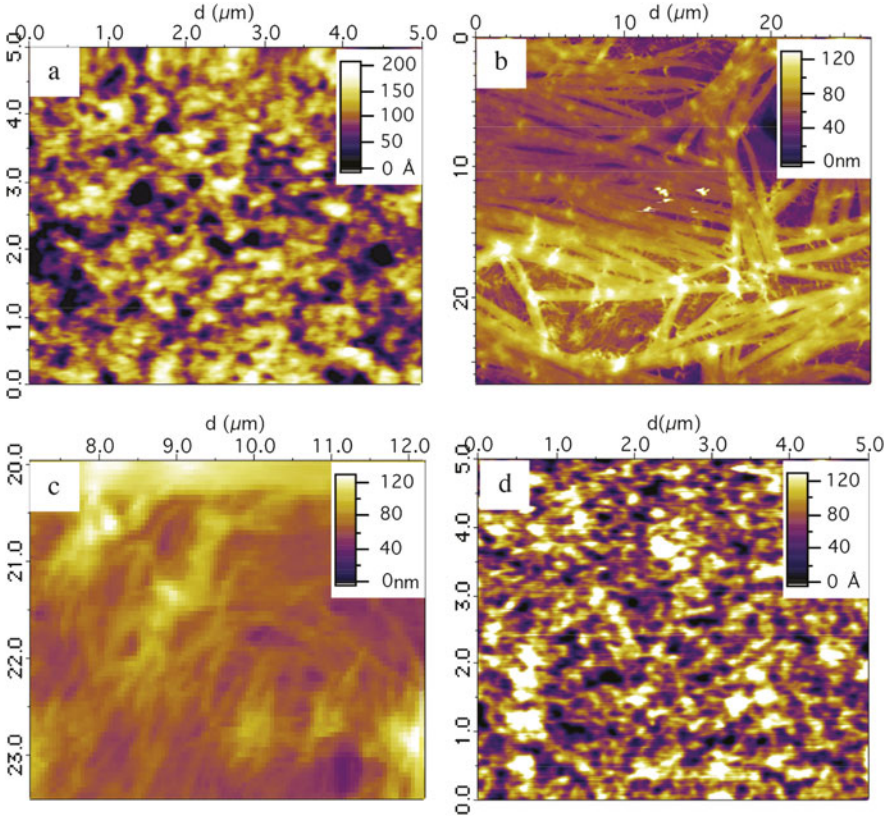

FIG. 3. AFM images of M5 (a), M9 (b), a zoomed section of M9 (c), and M17 (d).

yielding *d*-spacing on different length scales. Because of the polycrystalline nature of the samples and the resulting smeared diffraction patterns, it is impossible to reconstruct the atomic coordinates within a unit cell; however, the *a*, *b*, and *c* dimensions of the unit cell are obtainable and a packing structure can be proposed based on these results. A consequence of this is that while it is possible to identify how many molecules lie in a stack in the out-of-plane direction, for example, it is not possible to find exactly how the "corners" of the unit cell match up. Therefore, these stacks are considered in terms of molecular layers with a well-defined unit cell *a* dimension and repeating in-plane motifs with respective lengths of *b* and *c*, rather than attempting to piece together individual molecules in an exact fashion within a unit cell.

The out-of-plane GIWAXS reflections of M9 and M17 are associated with the *d*-spacing of the width of the oligomer backbone, perpendicular to both the π-stacking and backbone length dimensions, which for convenience is referred to as the "side-chain direction." This direction corresponds to the (*h*00) scattering peaks in the GIXRD data (Figs. 4 and 5) and the *a* dimension in the unit cell (Fig. 6). The M9 shows even and odd (*h*00) peaks, while M17 only shows even (*h*00) peaks. This discrepancy is discussed in detail in this section. The out-of-plane unit-cell *d*-spacing for M9 is 3.11 nm and for M17 is 3.09 nm, which is slightly less than twice the calculated oligomer width with extended aliphatic side chains (Fig. 2), indicating a two-layer unit cell with intercalation of the hexyl side chains. The presence of Bragg overtones indicates a lamellar stacking structure for both molecules.

These out-of-plane signals are expected to appear at the same positions for M9 and M17, because the two oligomers have the same width along the side-chain direction. In fact, the diffraction patterns do coincide, except that the Bragg reflections of M17 are located only at the positions of the even-order reflections of M9 [Fig. 5 (a)]. Likewise, though M9 diffracts signals at the odd-ordered reflections, these peaks are lower in intensity compared to the even-ordered reflections. This observation suggests a systematic packing effect upon the odd-ordered diffraction signals in both molecules. The alternating weaker and stronger intensities in the out-of-plane reflections for M9 indicate a slight break in the symmetry of the electron density profile of neighboring stacked molecular layers, which causes a partial disappearance of the weaker signals. This feature is attributed to the d-spacing of a two-molecule stack, but subsequent odd-ordered peaks are weakened. Additionally, the more intense, even-ordered peaks correspond approximately to a single oligomer's width in the side-chain direction. The intense reflections in these peaks suggest that diffraction

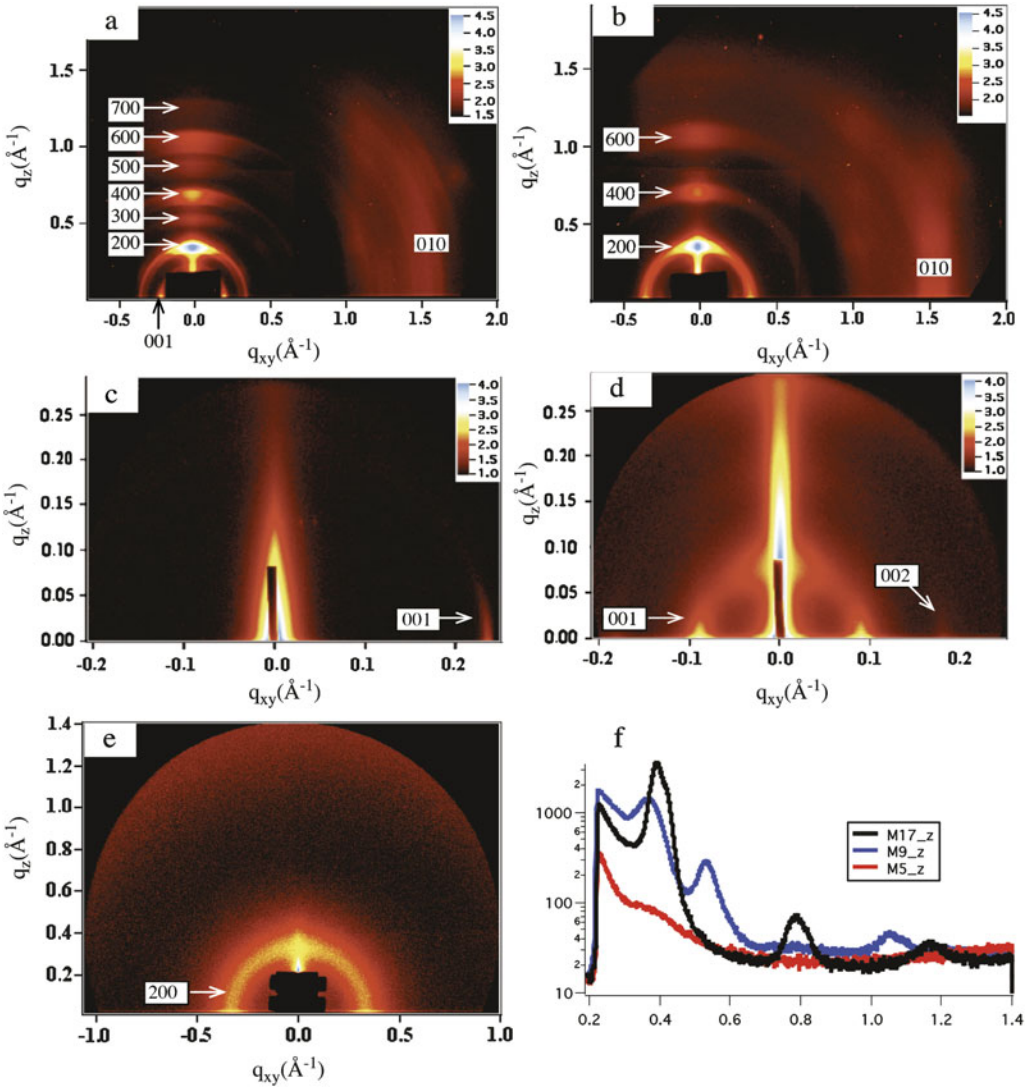

FIG. 4. GIWAXS and GISAXS diffraction images of M9 (a), (c), M17 (b), (d), and M5 (e), respectively. M17 indexing assumes a two-molecule unit cell. The color scale denotes the $\log_{10}$ x-ray reflection intensity. M5 shows a lack of structure, and the only dominant peak is an isotropic backbone length feature. The Bragg overtones in the q_z profiles of M9 and M17 in (f) indicate that these oligomers have order outside the unit cell, while the lack of overtones in M5 shows that the sample has no systematic order in this scale.

is occurring off of adjacent molecular layers. However, if the unit cell was only one molecular layer long in the *a* direction, as implied by diffraction off of adjacent molecular layers, then the odd-ordered peaks would be completely absent. The even-ordered peaks, therefore, have a partial contribution from diffraction of neighboring layers in the stack, plus an overlapping contribution from the Bragg overtones of the two-layer unit cell in the same direction. The odd-ordered peaks originate from a slight break in the adjacent layer symmetry, which causes a two-layer unit cell to be the smallest dimension that is repeatable by translation in the lattice, while nonetheless preserving a nearly identical electron density profile between adjacent layers. This is possible because most of the electron density is concentrated along the backbone, and the backbone is relatively invariant upon 180° rotation about the backbone axis. As a result, the out-of-plane diffraction signals are rationalized by adjacent stacking layers with oppositely directed ester chains. For example, if one layer's ester chains point toward the silicon substrate, then its neighboring layers have ester chains pointing away from the substrate. In this fashion, the out-of-plane pattern is repeated upon two-layer translation; and the electron density profiles of adjacent molecular layers are only slightly different from each other because the backbone position is similar, though not identical, no matter in which direction the ester chain points.

In the case of M17, the odd-ordered peaks are completely absent, which could imply either (i) that the oligomers form a well-ordered aggregate with the ester

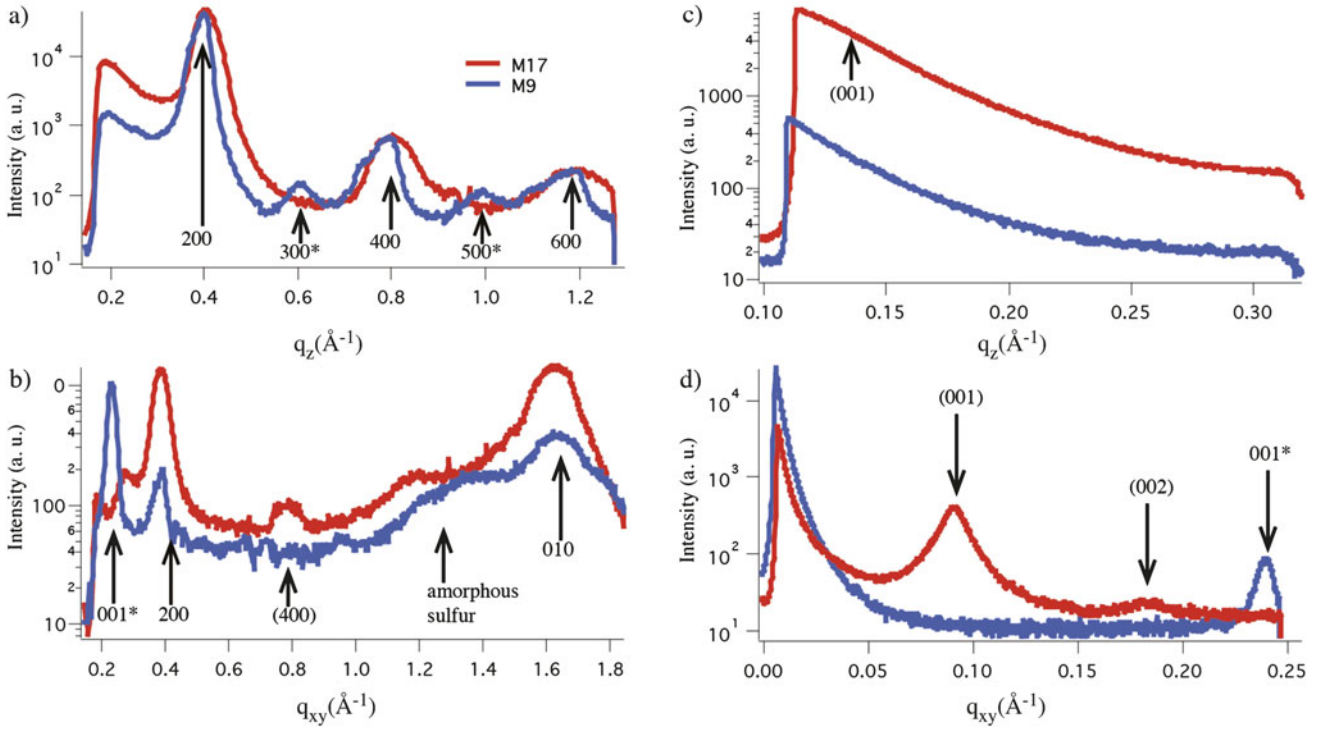

FIG. 5. Out-of-plane (a), (c) and in-plane (b), (d) line cuts from GIWAXS (a), (b) and GISAXS (c), (d) of M9 and M17, with indices. Asterisks signify that the peak only occurs in M9, and parentheses indicate the peak only occurs in M17. Unmarked indices occur in both samples.

chains pointing uniformly in the same direction, forming a one-layer unit cell or (ii) that the longer oligomer backbone causes an aggregation effect that prevents the diffraction from differentiating between adjacent layers, even though the M9 stacking pattern still approximately applies to the M17 case. In the long-backbone limit, it is reasonable to take P3HT as a first-order approximation of how the M series will aggregate, because at long lengths the M series and P3HT are identical except for a central thieno[3,4-b]thiophene ester defect. In P3HT thin films, the *a* dimension corresponds to one molecular layer along the side-chain direction, and the Bragg overtone peak intensities decay monotonically.[26] Therefore, at a glance the diffraction signals for M17 and P3HT coincide well. However, it is difficult to apply the M17 case directly to the P3HT one, because P3HT is symmetric along the side-chain axis. As a consequence, P3HT is impossible to flip to create an orientational defect. Therefore, if M17 takes on the pattern of P3HT, this implies the additional complication that all the esters must point in the same direction for the unit cell to be one layer wide in the side-chain axis. It is unlikely that this is the case, because the M9 shows that the M series has a proclivity to stack with ester chains facing each other, and, while the smaller relative abundance of the ester chain in M17 may affect sterics, it is unlikely that it would do so by sharply orienting half the layers in the opposite direction relative to M9. In order for M17 to take on an analogous aggregation condition to P3HT, the layers would instead have to contain orientational defects in which the ester chain points in the opposite direction than the pattern indicates. As a result, the layers become statistically averaged in the experiment, and therefore indistinguishable from one another to the x-ray diffraction. This also coincides with the notion that a longer oligomer backbone causes the ester chain to behave like a molecular defect: rather than inducing a well-aligned, fundamentally different aggregation pattern from M9, instead it causes increased orientational defects as a result of the decreased importance of the ester chain to the self-assembly process. Therefore, while the ester chain more tightly regulates the self-assembly characteristics in M9, in M17 it imposes an asymmetry and acts as a disruptor of order along the side-chain axis. As a result, the reflections corresponding to the two-layer unit cell disappear, and only the one-layer unit cell reflections appear. Nonetheless, the peaks are assigned (200), (400), and so on using the M9 indices, because this argument suggests that the M17 still aggregates the same way as M9 before orientational defects are considered. The increased orientational defects in M17 indicate that the ester chain interactions in the side-chain axis are weaker relative to M9, where the assembly is more ordered.

Diffraction features associated with π-stacking along the in-plane direction appear at $q = 1.61$ Å^{-1} for M9 and 1.65 Å^{-1} for M17, or $d = 0.39$ and 0.38 nm, respectively. In both samples, this feature occurs predominantly in the in-plane direction, which indicates an edge-on orientation

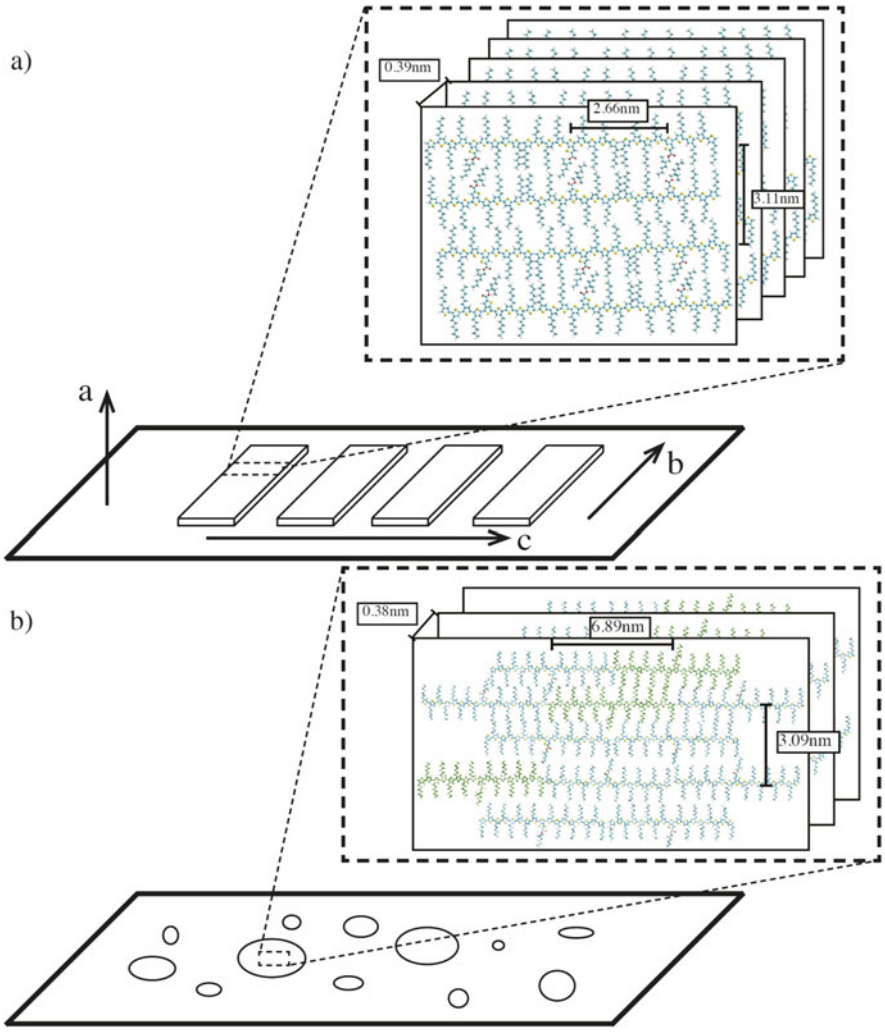

FIG. 6. An illustration of the molecular packing for M9 (a) and M17 (b), marked with unit-cell dimensions obtained from GIXRD data. The M9 surface morphology shows fibers oriented in a single direction, but actually fibers are oriented in many directions along the substrate surface. While these images show typical orientations for both molecules, the M17 film contains defects (colored green), which orient a molecule such that the ester is pointing in the opposite direction from the pattern norm. The M17 *a* stacking distance assumes a two-layer unit cell.

of these oligomers on the substrate (Fig. 6). Both samples have a broad feature underlying this π-stacking diffraction pattern, which is attributed to amorphous thiophene stacking.[26] M17 has a greater orientational distribution of this feature, indicated by the broad semicircular pattern centered at approximately $q = 1.6$ Å^{-1} in Fig. 4(b), which further substantiates the claim that M17 has increased orientational defects relative to M9. In contrast, this feature is not as fully semicircular in M9, suggesting that M9 has a more epitaxial orientation upon the substrate.

The M17 in-plane signal at $q = 0.0911$ Å^{-1} in the GISAXS image denotes a *d*-spacing of 6.89 nm, which is close to the calculated oligomer backbone length of 6.9 nm. M9 shows an in-plane signal in both GIWAXS and GISAXS at $q = 0.236$ Å^{-1}, which corresponds to a *d*-spacing of 2.66 nm. This feature corresponds approximately to the length of the M9 backbone. Therefore, both M17 and M9 lie with their backbones parallel to the substrate surface. While M17 has less than two times the number of monomer segments as M9, the *d*-spacing along the backbone for M17 is greater than two times the *d*-spacing of M9. This indicates that the backbone of M17 is more stretched, while the M9 backbone is more compressed. The M5 diffraction signal [Fig. 4(e)] shows a lack of regular order, displaying only a single isotropic ring at $q = 0.341$ Å^{-1} ($d = 1.84$ nm) corresponding to the side-chain axis, with no Bragg overtones unlike the M9 and M17 cases. This is consistent with the observation by eye that the M5 films beaded up shortly after preparation and were not expected to exhibit epitaxial crystallization. Figure 4(f) overlays q_z linecuts for M5, M9, and M17, to emphasize the lack of Bragg overtones in M5 relative to the other oligomers. This diffraction pattern is consistent

with ester–ester interactions between M5 molecules, but disorder among the distribution of M5 pairs.

The differences in the film morphology in the M series oligomers observed in the AFM results can be rationalized through the GIXRD results. As observed in these studies, the molecular self-assembly in films is driven by high affinities between moieties that are alike, such as between aromatic backbones, between aliphatic side chains and between ester groups. The end results of assembly are determined by the interplay between these different interactions. When one kind of moiety increases in relative abundance, the interactions between moieties of that type can overwrite other interactions. For instance, this is why M17 exhibits a larger occurrence of orientational defects because, as the T backbone length increases, the ester chain intermolecular contribution becomes smaller in proportion to the overall intermolecular interactions. Low molecular weight organic molecules under mainly van der Waals contributions are held together by many very low-energy interactions, typically individually on the order of single-digit kJ/mol.[9] Therefore, changes in functional group, molecular symmetry, charge distribution, etc. alter the packing structure. For the M series, the dominant themes of the intermolecular aggregations—the π-conjugated backbone facilitating π-stacking and making the molecules flat, aliphatic chains aggregating together, the ester chain sterics, and Van der Waals interactions—are conserved by the similarity of the molecules, since they differ only by backbone length. However, the relative abundance of each of these features within a single molecule, which is dependent on backbone length, also plays a fundamental role in the morphology. The M17 has more orientational defects because it has more abundant thiophene and hexyl moieties which, as they become more numerous, dominate the intermolecular contributions from other features in the molecule, such as the ester chain.[6] Additionally, as backbone length increases, the TT is reduced to just one of an increasing number of local defects in the oligomers. As a result, as backbone length increases, the ester chain imposes a less significant contribution to self-assembly. Also, because the additional aliphatic side chain and π-stacking interactions impose a more symmetric intermolecular stacking behavior than an ester chain appearing on just one side of the oligomer, M17 is more likely than M9 to exhibit orientational defects in the unit cell, where an oligomer is flipped in the incorrect direction. The result of the greater degree of orientational control in M9 relative to M17 is that M9 forms a fiber morphology upon spin coating, while M17 forms a dispersed morphology.

Figure 6 shows the proposed packing structure of the M9 and M17 two-molecule unit cells. Figure 6(b) assumes that the two-layer unit cell is the correct assignment for M17, i.e., that the first visible out-of-plane peak is indexed as (200) for reasons described previously. Therefore, we propose the following explanation for the backbone length dependent self-assembly characteristics. In the side-chain direction, the strength of the ester chain interaction depends on the relative abundance of the ester chain in the molecule. Therefore, M5 has the strongest ester chain interactions, followed by M9, and lastly M17. This is evident in the beaded-up assemblies of M5, where the interactions of M5 are strong enough to outcompete the interaction with the substrate surface. M9 is an intermediate case where the ester interactions no longer outcompete the surface tension, and therefore the M9 spreads out over the substrate. However, it does not spread out uniformly and instead forms aggregates with ester chains regularly oriented toward each other in adjacent stacking layers. The regular order of the ester chains, facing toward each other, indicates that the ester chains still impose a significant intermolecular interaction, though not as strong as in the M5 case. In the M17 case the ester chain contributions are the weakest, and therefore the ester interactions are not strong enough to prevent the oligomers from exhibiting orientational defects along the side-chain axis. At the same time, the opposite trend takes place in the π-stacking and aliphatic chain interactions, which are strengthened with increasing numbers of hexylthiophene monomers in the backbone. Therefore, M17 has the strongest π-stacking and aliphatic chain interactions, followed by M9, and lastly M5. As a result, M17 has less selective aggregation than M9, resulting in greater orientational variation, as evidenced by the increased semicircular diffraction pattern in the GIXRD data relative to M9 (Fig. 4). This is because the self-assembly interactions, compared with solution interactions, are strong enough that M17 molecules do not have to be well oriented with respect to one another to assemble; i.e., they are more forgiving to defects. It has been shown that the relative interplay of substrate, solution, and solute interaction energies will affect the aggregation patterns upon dewetting.[27] The M9 again represents an intermediate case, where the π-stacking is too weak to self-assemble without regard to orientation, but instead is more selective about how incoming oligomer recruits attach onto the growing crystal. As a result, M9 exhibits long (>26 μm) and short (~1 μm) fiber dimensions and epitaxial growth on the substrate surface. Also, in the case of M5, we propose that the π-stacking is weak enough that the ester chain interaction dominates the self-assembly. This is the reason M5 beads up into aggregates that lack crystallinity outside of the (200) feature, because the ester chain interactions are floppy relative to π-stacking and therefore do not promote an ordered crystalline structure in M5 films. As a result, the M5 does not diffract well, unlike the M9 and M17. This interplay of both stronger and weaker intermolecular interactions, arising from the relative abundances of important moieties, contributes to the different self-assembly characteristics in the M series. The well-balanced case between these orthogonal interactions exhibited the best

scenario for well-structured morphologies to form, while extremes in any one type of interaction led to a scattered morphology.

These results have significant implications for future low band gap organic materials. M17 was more P3HT-like, forming a smoother, more even film than M9. M9, because of a proper balance of competing intermolecular contributions, formed well-defined structures. On the other hand, M5 exhibited such strong intermolecular interactions from the dominant ester chain that it beaded up on the substrate and therefore would not be useful for thin films. The systematic investigation of these oligomers represents a preliminary step in the process of understanding how substitutions in the backbone and side chains of benchmark organic semiconducting polymers, as well as modulation of fragment length, can lead to systematically different self-assembly properties. This consideration is increasingly important as conjugated polymer studies trend toward low band gap materials, which are often realized by substituting along the backbone and side chains of benchmark polymers. These trends are useful from a device engineering standpoint as well, because different morphologies are better suited for different applications. The more even morphology of M17 is better suited to OPV applications, because the greater surface coverage presents a larger surface area for photon absorption. However, for an application that makes use of fiber morphologies, such as OFETs, M9 would be more ideal.

IV. CONCLUSION

A systematic structural study was carried out on the thin-film aggregation characteristics of a novel oligohexylthiophene system containing a central thieno[3,4-b] thiophene ester unit and oligomers varying by backbone length. AFM indicated that M9 forms fibers, while M5 and M17 form featureless aggregates. GIWAXS and GISAXS experiments were performed to describe the packing motifs of these oligomers and find the cause for this difference in aggregation behavior. The results of these studies indicate that M9 and M17 had orthorhombic unit cells containing two-layer stacks, oriented such that the esters alternate pointing toward or away from the substrate on a layer-by-layer basis. On the other hand, M5 evidenced a lack of regular order due to the high relative abundance of the ester chain within the molecule. The presence of orientational defects resulting from a smaller relative abundance of the ester chain, coupled with an increased π-stacking strength, was determined to be responsible for the dispersed morphology in M17 films. Meanwhile, the balance of ester and π-stacking strength in M9 was responsible for the tendency to form crystalline fibers.

Therefore, the contributions from the oligomer backbone, π-stacking, hexyl chain interactions, and ester chain impose very different morphologies upon oligothiophene derivatives of varying backbone lengths. For longer oligomers, the ester chain becomes more like a molecular defect than a regularly orienting feature, which causes a dispersed morphology of random domains across the film. A common theme in these oligomers is that the ester chain causes asymmetry along the side-chain axis profile. While the benchmark polymer P3HT is symmetric along the side-chain axis and therefore in the past often this asymmetry has not presented itself as an issue, the design strategies of organic photovoltaics have turned to low band gap polymers. Compounds of increasing complexity, fragment length variation, and asymmetry relative to P3HT are being developed to improve organic semiconductor device characteristics.[1] As a result, new difficulties are arising, because all of these strategies have self-assembly as well as photophysical consequences, and the optimization of one often generates problems for the other. Therefore, it is important to understand how the length-dependent aggregation characteristics are being impacted by these alterations. This study therefore represents a preliminary step in the understanding of how substitutions into the side chains and oligomer backbone of benchmark polymer derivatives affect active layer self-assembly, which has strong implications upon the PCE of organic semiconductor devices.

ACKNOWLEDGMENTS

This work is supported as part of the ANSER Center, an Energy Frontier Research Center funded by the U.S. Department of Energy, Office of Science, Office of Basic Energy Sciences, under Award No. DE-SC0001059. The Setup fund from Northwestern University to L.X.C. provided partial support of this research. We would also like to thank Dr. Sonke Seifert for his technical support. The use of the Advanced Photon Source was supported by the U.S. Department of Energy, Office of Science, Office of Basic Energy Sciences, under Contract No. DE-AC02-06CH11357.

REFERENCES

1. Y. Liang, D. Feng, J. Guo, J.M. Szarko, C. Ray, L.X. Chen, and L. Yu: Regioregular oligomer and polymer containing thieno [3,4-b]thiophene moiety for efficient organic solar cells. *Macromolec.* **42**, 1091 (2009).
2. G. Dennler, M. Scharber, and C. Brabec: Polymer-fullerene bulk-heterojunction solar cells. *Adv. Mater.* **27**, 1 (2009).
3. S. Holdcroft: Patterning π-conjugated polymers. *Adv. Mater.* **13**, 7154 (2001).
4. R.H. Friend, R.W. Gymer, A.B. Holmes, J.H. Burroughes, R.N. Marks, C. Taliani, D. Bradley, D.A.D. Santos, J.L. Brédas, M. Lögdlund, and W.R. Salaneck: Electroluminescence in conjugated polymers. *Nature* **397**, 121 (1999).
5. A.C. Mayer, M.F. Toney, S.R. Scully, J. Rivnay, C. Brabec, M. Scharber, M. Koppe, M.H. McCulloch, and M.D. McGehee: Bimolecular crystals of fullerenes in conjugated polymers and the

implications of molecular mixing for solar cells. *Adv. Funct. Mater.* **19**, 1173 (2009).
6. G.R. Desiraju: Crystal engineering: A holistic view. *Angew. Chem.* **46**, 8342 (2007).
7. M.C. Etter: Encoding and decoding hydrogen-bond patterns of organic compounds. *Acc. Chem. Res.* **23**, 120 (1990).
8. A. Gavezzotti: *Molecular Aggregation: Structure Analysis and Molecular Simulation of Crystals and Liquids* (Oxford University Press, New York, NY, 2007), pp. 367–418.
9. J.N. Israelachvili: *Intermolecular and Surface Forces* (Academic Press, San Diego, CA, 1995).
10. M. Dante, J. Peet, and T. Nguyen: Nanoscale charge transport and internal structure of bulk heterojunction conjugated polymer/fullerene solar cells by scanning-probe microscopy. *J. Phys. Chem. C* **112**, 7241 (2008).
11. L. Pingree, O.G. Reid, and D. Ginger: Electrical scanning-probe microscopy on active organic electronic devices. *Adv. Mater.* **21**, 19 (2009).
12. J. Peet, J.Y. Kim, N.E. Coates, W.L. Ma, D. Moses, A.J. Heeger, and G.C. Bazan: Efficiency enhancement in low-bandgap polymer solar cells by processing with alkane dithiols. *Nat. Mater.* **6**, 497 (2007).
13. I. Hwang, D. Moses, and A. Heeger: Photoinduced carrier generation in P3HT/PCBM bulk heterojunction materials. *J. Phys. Chem. C* **112**, 4350 (2008).
14. M.J. Winokur, D. Spiegel, Y. Kim, S. Hotta, and A.J. Heeger: Structural and absorption studies of the thermochromic transition in poly(3-hexylthiophene). *Synth. Met.* **28**, C419 (1989).
15. A. Gavezzotti and G. Filippini: Crystal packing and lattice energies of polythienyls: Calculations and predictions. *Synth. Met.* **40**, 257 (1991).
16. R. Azumi, M. Goto, K. Honda, and M. Matsumoto: Conformation and packing of odd-numbered alpha-oligothiophenes in single crystals. *Bull. Chem. Soc. Jpn.* **76**, 1561 (2003).
17. J. Cornil, D. Beljonne, J. Calbert, and J. Brédas: Interchain interactions in organic p-conjugated materials: Impact on electronic structure, optical response, and charge transport. *Adv. Mater.* **13**, 1053 (2001).
18. D. Fichou: Structural order in conjugated oligothiophenes and its implications on opto-electronic devices. *J. Mater. Chem.* **10**, 571 (2000).
19. J. Lehn: Toward self-organization and complex matter. *Science* **295**, 2400 (2002).
20. A. Schenning and E. Meijer: Supramolecular electronics: Nanowires from self-assembled π-conjugated systems. *Chem. Commun.* 3245 (2005).
21. J. Guo, Y. Liang, J. Szarko, B. Lee, H.J. Son, B.S. Rolczynski, L. Yu, and L.X. Chen: Structure, dynamics, and power conversion efficiency correlations in a new low bandgap polymer: PCBM solar cell. *J. Phys. Chem. B* **114**, 742 (2010).
22. J.M. Szarko, B.S. Rolczynski, J. Guo, Y. Liang, F. He, M.W. Mara, L. Yu, and L.X. Chen: Electronic processes in conjugated diblock oligomers mimicking low band-gap polymers: Experimental and theoretical spectral analysis. *J. Phys. Chem. B* **114**, 14505 (2010).
23. D. Beljonne, Z. Shuai, G. Pourtois, and J.L. Bredas: Spin-orbit coupling and intersystem crossing in conjugated polymers: A configuration interaction description. *J. Phys. Chem. A* **105**, 3899 (2001).
24. M. Chabinyc: X-ray scattering from films of semiconducting polymers. *Pol. Rev.* **48**, 463 (2008).
25. Y. Kim, S. Cook, S.M. Tuladhar, S.A. Choulis, J. Nelson, J.R. Durrant, D.D.C. Bradley, M. Giles, I. McCulloch, C-s. Ha, and M. Ree: A strong regioregularity effect in self-organizing conjugated polymer films and high-efficiency polythiophene: Fullerene solar cells. *Nat. Mater.* **5**, 198 (2006).
26. S. Joshi, S. Grigorian, and U. Pietsch: X-ray structural and crystallinity studies of low and high molecular weight poly(3-hexylthiophene). *Phys. Status Solidi, A Appl. Mater. Sci.* **205**, 488 (2008).
27. A. Raudino and B. Pignataro: Supra-aggregates of fiber-forming anisotropic molecules. *J. Phys. Chem. B* **110**, 2116 (2006).